New chemical tools to illuminate N-acylphosphatidylethanolamine biosynthesis

Wendel, T.J.

3

Biochemical profiling of the novel PLA2G4E inhibitor WEN091

Phospholipase A2ε (PLA2G4E) is a serine hydrolase that belongs to Group IV of the phospholipase A_2 family. It has five closely related family members (A–D and F), which share structural similarity despite their relatively low amino acid homology (30% on average).[1] These isozymes have PLA_1, PLA_2, lysophospholipase and acyltransferase activity *in vitro*, but have distinct preferences and calcium-dependencies.[2,3] They are characterized by the presence of an N-terminal calcium-binding C2 domain (apart from PLA2G4C) and an unconventional Ser-Asp catalytic dyad in their lipase domain.[4,5] PLA2G4E was recently proposed to be the enzyme responsible for the Ca^{2+}-dependent biosynthesis of *N*-acylphosphatidylethanolamines (NAPEs) in the brain.[6] It acts as an *N*-acyltransferase (NAT) transferring the *sn*-1 *O*-acyl substituent from phosphatidylcholine (PC) to the free amine of phosphatidylethanolamine (PE) (Figure 3.1).[6,7]

NAPEs are an underexplored class of lipids with both structural and signaling functionalities. NAPEs are low-abundant but widely found across species and tissues.[8,9] They provide rigidity to cellular membranes[10,11], are involved in cation-dependent membrane fusion[12] and influence the localization of membrane-interacting proteins.[13,14] In addition, NAPEs have anorectic and anti-inflammatory signaling functions.[15–17] Beside the Ca^{2+}-dependent pathway, Ca^{2+}-independent NAPE biosynthesis is performed by NAT activity of phospholipase $A_{1/2}$/acyltransferase (PLAAT) enzymes 1–5.[18,19] NAPEs are converted into *N*-acylethanolamines (NAEs) either directly by NAPE-specific phospholipase D (NAPE-PLD) or via one of several multistep pathways (Figure 3.1).[20–23] The first of these alternative pathways includes *sn*-2 ester hydrolysis to lyso-NAPEs by α/β hydrolase domain-containing protein 4 (ABHD4) or other PLA_2-type enzymes.[24] Lyso-NAPEs are then converted to NAEs by PLD-type activity of glycerophosphodiesterase 4 (GDE4) or GDE7.[21,25] Alternatively, ABHD4 hydrolyzes the *sn*-1 ester producing glycerophospho-NAEs (GP-NAEs), which are then converted to NAEs by GDE1.[26] Third, NAEs can be biosynthesized via PLC-type hydrolysis of NAPEs to phospho-NAEs and sequential dephosphorylation.[24,27] Of note, plasmalogen-type NAPEs (pNAPEs) bear an *sn*-1 ether, which cannot be hydrolyzed by ABHD4. Metabolism of pNAPEs to NAEs is therefore restricted to the other three pathways (Figure 3.1B).[23] NAEs are a diverse family of signaling lipids that are involved in a plethora of physiological functions, depending on their *N*-acyl substituent, including inflammation, nociception and satiety.[28–32] *N*-Arachidonoylethanolamine (AEA or anandamide) is an endocannabinoid, regulating neurotransmission, memory formation, fertility and stress, among others, via activation of cannabinoid receptor 1 (CB_1).[32–36] The activity of NAEs is terminated by fatty acid amide hydrolase (FAAH) or *N*-acylethanolamine acid amidase (NAAA).[37,38] Following acute brain ischemia both NAPEs and NAEs are dramatically increased, which is suggested to have a neuroprotective effect.[39–41] Since elevated intracellular calcium concentrations are a hallmark of ischemia[42], PLA2G4E activity might be pivotal in this response. Potent and selective inhibitors of PLA2G4E would therefore be valuable tools to elucidate the role of PLA2G4E in both basal and pathophysiological NAPE production.

In Chapter 2, compound screening and a hit optimization program led to the identification of **WEN091** as an inhibitor of PLA2G4E. In this chapter, the biochemical profile of **WEN091** was further explored in both *in vitro* and cellular assays.

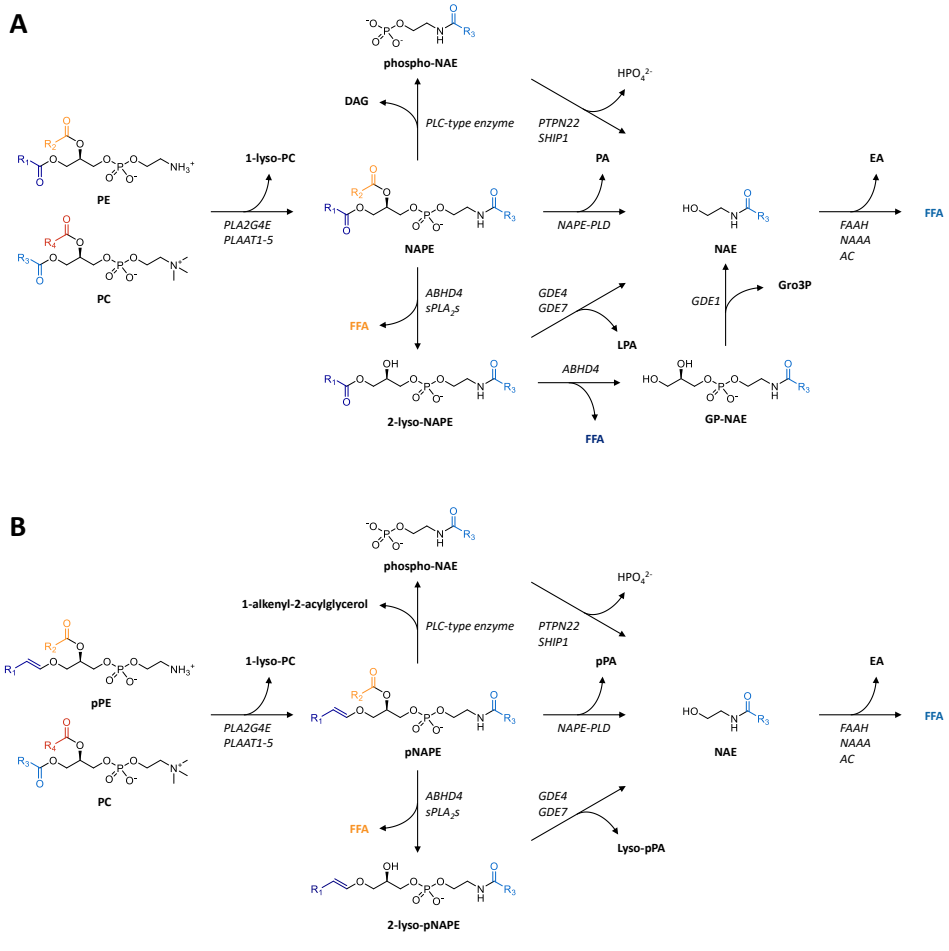

Figure 3.1. Pathways of NAPE and pNAPE metabolism. A) Acyl transfer from a donor lipid such as phosphatidylcholine (PC) to phosphatidylethanolamine (PE) by PLA2G4E or phospholipase/acyltransferase (PLAAT) 1–5 produces *N*-acyl-PE (NAPE), which is metabolized to *N*-acylethanolamine (NAE) either via direct phospholipase D (PLD) activity by NAPE-specific PLD (NAPE-PLD) or one of three multistep pathways involving sequential PLA_1, PLA_2, PLC, PLD and dephosphorylation reactions. B) Plasmalogen-type NAPE (pPE) are produced from plasmenylethanolamine (pPE). Metabolism of pNAPE is restricted to three possible pathways. ABHD4: α/β hydrolase domain-containing protein 4, PLA_2s: PLA_2-type enzymes, GDE: glycerophosphodiesterase, PTPN22: protein tyrosine phosphatase non-receptor type 22, SHIP1: Src homology 2 domain-containing inositol 5′ phosphatase 1, FAAH: fatty acid amide hydrolase, NAAA: NAE-hydrolyzing acid amidase, AC: acid ceramidase, PA: phosphatidic acid, LPA: lysophosphatidic acid, GP-NAE: glycerophospho-NAE, Gro3P: glycerol-3-phosphate, DAG: diacylglycerol, EA: ethanolamine, FFA: free fatty acid, pPA: plasmenic acid. R = saturated, mono- or polyunsaturated fatty acyl.

Results

Activity on human and mouse PLA2G4E and related enzymes

Competitive activity-based protein profiling (cABPP) is a powerful chemical biology technique to assess the activity and selectivity of enzyme inhibitors in complex proteomes. Competitive ABPP makes use of fluorescently tagged activity-based probes (ABPs), such as fluorophosphonate-tetramethylrhodamine (FP-TAMRA) that reacts in a covalent manner with the nucleophilic serine in the active site of serine hydrolases. Here, cABPP was used to determine the activity of **WEN091** on recombinant human PLA2G4E expressed in human embryonic kidney 293 (HEK293T) cells. In brief, lysates from HEK293T cells overexpressing recombinant human or mouse PLA2G4E were preincubated with various concentrations of **WEN091** or vehicle for 30 min at room temperature followed by 50 nM FP-TAMRA for 5 min. Proteins were resolved by molecular weight using sodium dodecyl sulfate–polyacrylamide gel electrophoresis (SDS-PAGE) and subsequent in-gel fluorescence scanning allowed quantification of enzyme labeling and inhibition thereof by **WEN091**. **WEN091** inhibited hPLA2G4E, with an apparent half maximal inhibitory concentration (IC_{50}) of 10 nM (pIC_{50} ± SEM = 8.01 ± 0.02) (Figure 3.2A–C). Preliminary experiments indicated that **WEN091** was also active on mouse PLA2G4E (pIC_{50} = 6.87 ± 0.07) (Supplementary Figure S3.1). Next, the inhibitory activity of **WEN091** was investigated using a liquid chromatography-mass spectrometry (LC-MS)-based natural

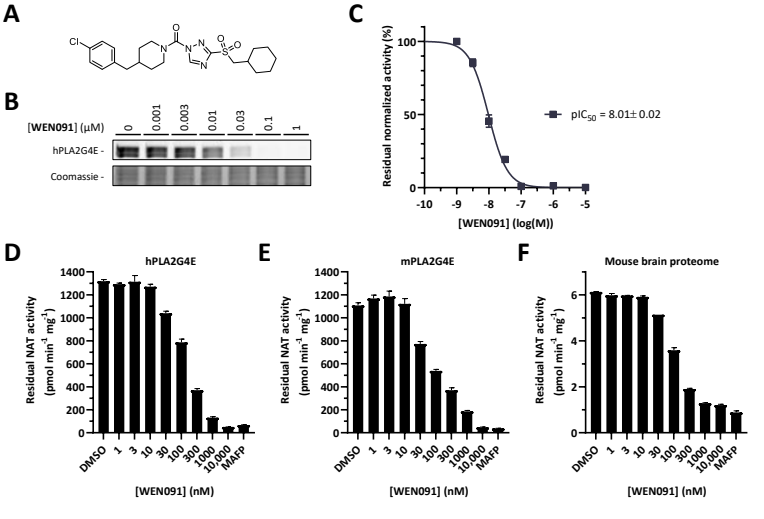

Figure 3.2. WEN091 is a potent inhibitor of PLA2G4E. A) Chemical structure of WEN091. B) Representative gel excerpts of cABPP experiments on hPLA2G4E overexpression lysate, using FP-TAMRA. C) Inhibition curve and pIC_{50} value corresponding to the cABPP experiment in B. Data presented as mean ± SEM (N = 2). D–F) Dose-dependent inhibition by **WEN091** of NAPE formation from 1,2-dipalmitoyl-PC and 1,2-dioleoyl-PE in human (D) or murine (E) PLA2G4E-overexpression lysate or mouse brain proteome (F). Methyl arachidonoyl-FP (MAFP) was used as control. Bars represent mean ± SEM of conversion rate determined using LC-MS/MS (N = 2).

substrate assay. In line with the gel-based cABPP assay results, **WEN091** dose-dependently inhibited *N*-palmitoyl-*sn*-1,2-dioleoylphosphatidylethanolamine biosynthesis by recombinant human and mouse PLA2G4E and mouse brain homogenate, with pIC_{50} values of 6.87 ± 0.02 (hPLA2G4E), 7.09 ± 0.08 (mPLA2G4E) and 7.02 ± 0.01 (mouse brain proteome) (Figure 3.2D–F and Supplementary Figure S3.2). Altogether, these data indicate that **WEN091** is a potent inhibitor of PLA2G4E.

To determine **WEN091**'s selectivity over the other Group IV phospholipase members, a gel-based competitive ABPP assay was deployed (Figure 3.3A, B). Of note, the inhibition values determined using this approach are apparent IC_{50} and apparent selectivity values that can only be used to compare compounds that have been tested under identical conditions. **WEN091** showed inhibitory activity on mouse PLA2G4B (pIC_{50} = 6.65 ± 0.11) and mPLA2G4D (pIC_{50} = 5.85 ± 0.06), but no activity on human PLA2G4C (pIC_{50} < 5.0). Activity on PLA2G4A and F could not be determined due to lack of expression in the

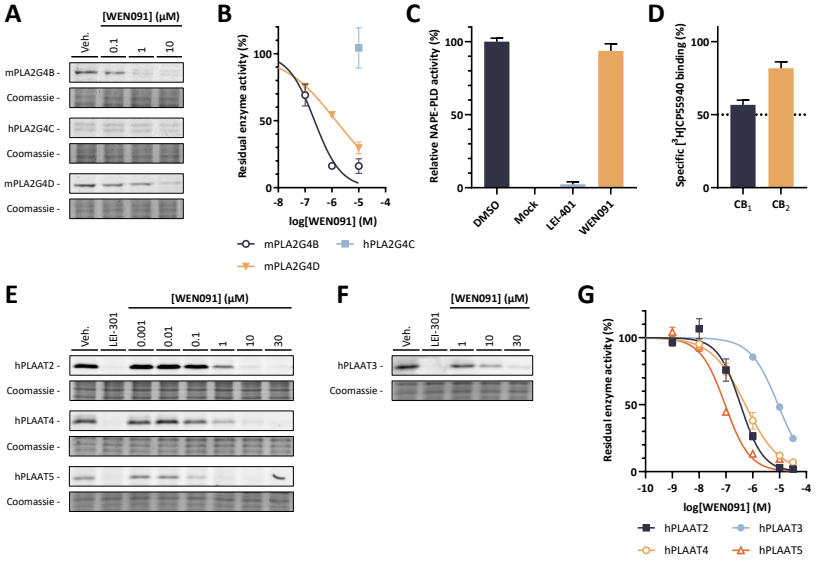

Figure 3.3. WEN091 is selective over other PLA2G4 enzymes and enzymes involved in NAPE metabolism. A) Representative gel excerpts of cABPP experiments on mPLA2G4B, hPLA2G4C or mPLA2G4D overexpression lysate, using FP-TAMRA. B) Inhibition curves of **WEN091** on PLA2G4B–D corresponding to the cABPP experiments in A). Data presented as mean ± SEM (N = 3). C) Activity of **WEN091** (10 µM) on NAPE-PLD in a fluorogenic substrate (PED6) assay on overexpression lysate. NAPE-PLD inhibitor LEI-401 (10 µM) was used as control.[43] Data presented as mean ± SEM (N = 2, n = 2). D) Displacement of radiolabeled ligand [^{3}H]CP55,9940 from CB_1 and CB_2 receptors by **WEN091** (10 µM) in overexpression lysate. Data presented as relative mean of DMSO control (100%) ± SEM (N = 3, n = 3). E–F) Representative gel excerpts of cABPP experiments on hPLAAT2, hPLAAT4, hPLAAT5 (E) or hPLAAT3 (F) overexpression lysate, using MB064 as ABP and pan-PLAAT inhibitor LEI-301 (10 µM) as control.[44] G) Inhibition curves of **WEN091** on hPLAAT2–5 corresponding to the cABPP experiments in E–F). Data presented as mean ± SEM (N = 2).

Table 3.1. Inhibition values of WEN091 on PLA2G4 enzymes and enzymes involved in NAPE metabolism. Inhibition values determined using gel-based cABPP (PLA2G4B–D, N = 3, PLAAT2–5, N = 2), PED6 assay (NAPE-PLD, N = 2, n = 2) or [^{3}H]CP55,940 displacement assay ($CB_{1/2}$, N = 3, n = 3) on overexpression lysate. Data reported as pIC_{50} ± SEM. When <50% inhibition or displacement was observed at 10 µM, % residual activity is reported.

Enzyme	PLA2G4B	PLA2G4C	PLA2G4D	PLAAT2	PLAAT3	PLAAT4	PLAAT5	NAPE-PLD	CB_1	CB_2
Inhibition	6.65	104	5.85	6.46	5.05	6.28	7.03	94	57	82
value	± 0.11	± 26%	± 0.06	± 0.07	± 0.02	± 0.05	± 0.07	± 10%	± 3%	± 4%

HEK293T cells. **WEN091** showed no activity on NAPE-hydrolyzing enzyme NAPE-PLD in a biochemical fluorescence-based assay[45] and did not potently bind to cannabinoid CB_1 and CB_2 receptors in a radiometric displacement assay[46] (Figure 3.3C–D, Table 3.1). In addition, activity on the PLAAT enzymes was assessed in a competitive gel-based ABPP assay.[44] At 10 nM (the hPLA2G4E IC_{50}), **WEN091** showed no significant inhibitory activity on PLAAT2–5, but at higher concentrations these enzymes were inhibited (Figure 3.3E–G, Table 3.1). The activity on PLAAT1 could not be determined due to lack of expression in the HEK293T cells. Thus, **WEN091** is a potent inhibitor of NAPE biosynthesis with a >10-fold preference for inhibition of the Ca^{2+}-dependent pathway of NAPE formation.

The selectivity of **WEN091** over other serine hydrolases in mouse brain proteome was determined using gel-based cABPP (Figure 3.4). **WEN091** appeared to be a selective PLA2G4E inhibitor at 10 and 100 nM (Figure 3.4), but inhibited several enzymes at higher concentrations, including α/β hydrolase domain-containing protein 6 (ABHD6), diacylglycerol lipase α (DAGLα), FAAH, acyl protein thioesterases 1 and 2 (LyPLA1/2) and carboxylesterases (CES) (Table 3.2). Using competitive chemical proteomics, which makes use of LC-MS/MS to accurately identify probe targets, the identity of the serine hydrolase off-targets was confirmed (Table 3.2, Supplementary Figure S3.3).

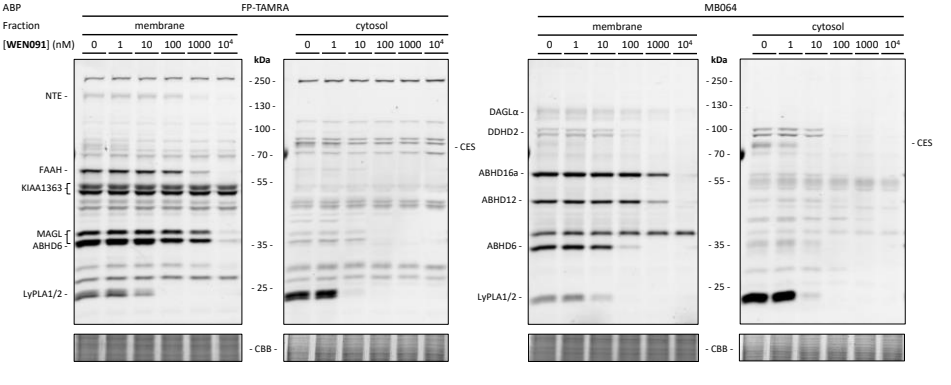

Figure 3.4. *In vitro* activity of WEN091 on mouse brain enzymes. Representative gel images of cABPP experiments on mouse brain membrane or cytosol proteome using FP-TAMRA or MB064. Several labeled serine hydrolases are indicated.

Table 3.2. Inhibition values of WEN091 on mouse brain enzymes. pIC_{50} values determined by cABPP experiments on mouse brain membrane or cytosol proteome (30 min, RT) using FP-TAMRA or MB064 (20 min, RT). Data presented as mean ± SEM (N = 3). The third column shows inhibition of these enzymes by **WEN091** (1 µM, 30 min, 37°C) as determined in a chemical proteomics experiment with FP-biotin (4 µM, 60 min, RT). Data presented as ratios of quantified peptides between **WEN091** and DMSO-treated samples (preliminary, N = 1). Minimal ratio was manually set to 0.05.

Enzyme	pIC_{50} ± SEM	Ratio WEN091/DMSO
ABHD6	7.89 ± 0.02	≤ 0.05
ABHD12	6.53 ± 0.04	≤ 0.05
ABHD16a	6.33 ± 0.04	0.12
CES	9.06 ± 0.03	≤ 0.05
DAGLα	6.51 ± 0.04	≤ 0.05
DDHD2	7.34 ± 0.04	0.07
FAAH	6.52 ± 0.04	≤ 0.05
KIAA1363	< 5.0	1.38
LyPLA1/2	8.27 ± 0.04	≤ 0.05
MAGL	5.89 ± 0.07	0.08
NTE	6.48 ± 0.06	0.31

Profiling the cellular activity of WEN091

Next, the cellular activity profile of **WEN091** was determined in mouse Neuro-2a cells using gel-based cABPP.[43,47–49] At 10 and 100 nM, **WEN091** inhibited ABHD6 (pIC_{50} = 8.56 ± 0.05), FAAH (pIC_{50} = 8.17 ± 0.07) and LyPLA1/2 (pIC_{50} = 7.83 ± 0.08, Figure 3.5 and Table 3.3). In addition, **WEN091** partially inhibited DDHD domain-containing protein 2 (DDHD2) and neuropathy target esterase (NTE) (pIC_{50} = 7.14 ± 0.08 and 7.13 ± 0.10, respectively). These results indicated that **WEN091** was able to cross the plasma membrane and inhibit intracellular enzymes. Compared to the mouse brain *in vitro* assay, the activity on FAAH was increased approximately 50 times, whereas the activity on DDHD2 and LyPLA1/2 was slightly reduced (approximately 2 and 3 times, respectively, Table 3.2 and Table 3.3). In line with the chemical proteomics results, **WEN091** inhibited several other serine hydrolases at higher concentrations, including ABHD12, ABHD16a and DAGLβ. PLA2G4E activity could not be detected in this assay. Thus, **WEN091** is a cellular active inhibitor, but has several serine hydrolase off-targets in living cells.

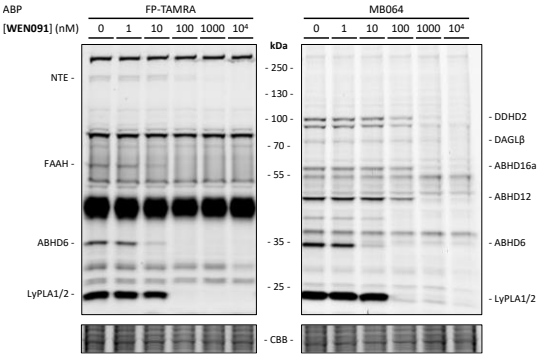

Figure 3.5. Cellular activity of WEN091 on Neuro-2a enzymes. Representative gel images of cABPP experiments on Neuro-2a cells using FP-TAMRA or MB064. Several labeled serine hydrolases are indicated.

Table 3.3. Inhibition values of WEN091 on Neuro-2a enzymes. Values determined by cABPP experiments on Neuro-2a cells using FP-TAMRA or MB064. Data presented as mean ± SEM (N = 3).

Enzyme	ABHD6	ABHD12	ABHD16a	DAGLβ	DDHD2	FAAH	LyPLA1/2	NTE
pIC_{50}	8.56	7.01	6.62	6.72	7.14	8.17	7.83	7.13
± SEM	± 0.05	± 0.04	± 0.07	± 0.25	± 0.08	± 0.07	± 0.08	± 0.10

To determine the functional effect of **WEN091** in living cells, recombinant hPLA2G4E was transiently overexpressed in Neuro-2a cells. Cells were harvested 24 h after transfection, lysed and the lipids were extracted. Targeted LC-MS/MS analysis revealed increased levels of NAPEs, lyso-NAPEs and NAEs, and to a lesser extent of plasmalogen-type NAPEs (pNAPEs) compared to mock-transfected cells (Figure 3.6A and Supplementary Figure S3.4). All analyzed NAPE levels were increased at least 4-fold, with *N*-palmitoyl (16:0) and *N*-oleoyl (18:1) species showing the largest increase up to 50-fold. NAE levels were all increased at least 2-fold, except *N*-docosahexaenoylethanolamine (DHEA, 22:6), which was not changed. *N*-stearoylethanolamine (SEA, 18:0) and *N*-docosatetraenoylethanolamine (DEA, 22:4) showed the largest accumulation of over 10-fold. Overexpression did not affect levels of lyso-pNAPEs, free fatty acids (FFAs) and glycerides. These results demonstrated that overexpressed PLA2G4E and NAPE-metabolizing enzymes are present and catalytically active in the Neuro-2a cells.

Next, the cells were treated with **WEN091** or **WEN258** (8 h, starting 24 h after transfection). **WEN258** is a structural analog of **WEN091** with a similar cellular selectivity profile but no activity on PLA2G4E (Figure 3.7, see also Chapter 4) and was used as a control-compound. **WEN091** dose-dependently lowered NAPE and lyso-NAPE levels up to ± 50% compared to DMSO-treated cells, whereas **WEN258** did not (Figure 3.6B, C for a cross-sectional selection of lipids and Supplementary Figure S3.5 for the full panel). Of note, levels of some NAPEs were increased after **WEN258** treatment, which might be due to inhibition of a NAPE-metabolizing enzyme. Interestingly, the levels of *N*-

docosahexaenoyl (*N*-22:6)-lyso-NAPEs were not increased upon PLA2G4E overexpression (Supplementary Figure S3.4B), but were by both **WEN091** and **WEN258** treatment (Figure 3.6C and Supplementary Figure S3.6). This may suggest that *N*-22:6 lyso-NAPEs are biosynthesized via a PLA2G4E-independent pathway and/or that these lipids are rapidly metabolized by a common off-target of **WEN091** and **WEN258**. Treatment with the inhibitors showed no significant effect on lyso-pNAPE levels, suggesting these lipids are metabolized independently of PLA2G4E and other targets of the compounds. Furthermore, **WEN091** did not significantly modulate NAE levels, but **WEN258** increased these (Figure 3.6D). This might be explained by inhibition of FAAH by both compounds (Table 3.3 and Figure 3.7), suggesting combined inhibition of PLA2G4E and FAAH by **WEN091** balances NAE levels. Finally, both compounds decreased GP-PEA, FFA and 2-AG levels, confirming PLA2G4E-independent activity of the inhibitors (Supplementary Figure S3.7). To conclude, **WEN091** is an inhibitor of PLA2G4E that lowered intracellular (lyso)-NAPE production, but has several off-targets that modulate other lipid species.

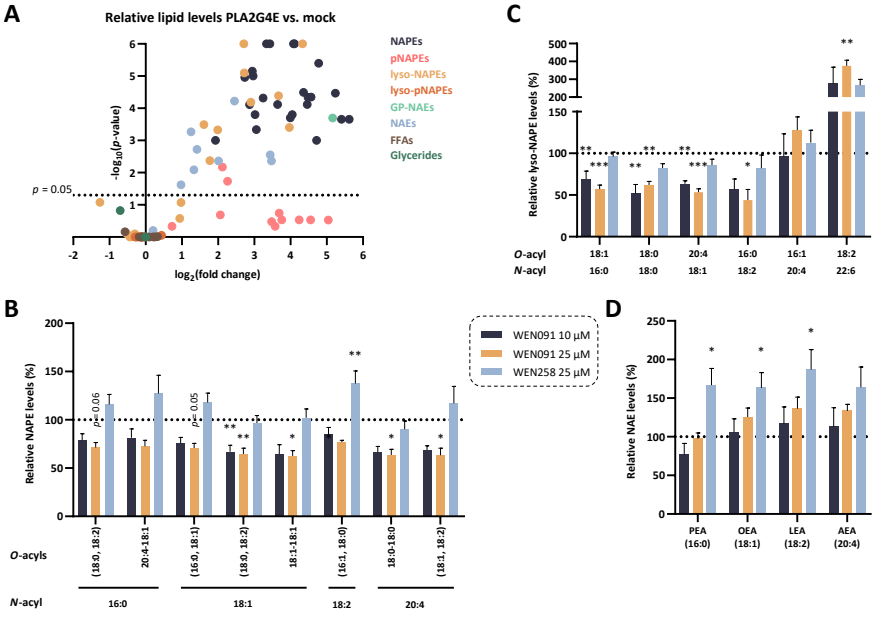

Figure 3.6. Lipid levels in Neuro-2a cells overexpressing PLA2G4E and following treatment with WEN091. A) Volcano plot of relative lipid levels in PLA2G4E-transfected vs. mock-transfected Neuro-2a cells (24 h p.t.). Statistical significance calculated for each lipid using a two-tailed *t*-test with Holm-Sidak multiple comparison correction. B-D) Effect of inhibitor or control compound treatment (8 h) on the levels of several NAPEs (B), lyso-NAPEs (C) and NAEs (D) in PLA2G4E-overexpressing Neuro-2a cells (24 h p.t.), expressed as relative levels compared to vehicle-treated cells (mean ± SEM, N = 5). Statistical significance calculated for each lipid using one-way ANOVA with Dunnett's multiple comparison correction. **p* < 0.05, ***p* < 0.01, ****p* < 0.001.

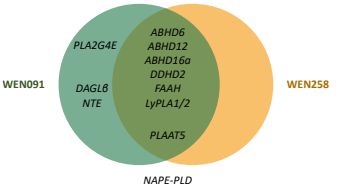

Figure 3.7. Selectivity profile of WEN091 and WEN258. Included are serine hydrolases identified in Neuro-2a cells and (human orthologs of) enzymes involved in mouse NAPE metabolism for which inhibition data of both inhibitors was obtained and that are inhibited at least 50% by 10 μM of inhibitor. For complete data of **WEN258**, see Chapter 4.

Discussion and Conclusion

In Chapter 2, **WEN091** was identified as the first potent inhibitor of PLA2G4E. Here, its activity was confirmed on the mouse ortholog, showing high potency in gel-based cABPP and biochemical assays using recombinant mPLA2G4E and endogenous PLA2G4E in mouse brain. **WEN091** was cellular active and inhibited the formation of NAPEs and lyso-NAPEs in PLA2G4E-overexpressing Neuro-2a cells, but did not affect NAE levels. It was selective over the cannabinoid receptors and NAPE-PLD, but unexpectedly inhibited PLAAT2–5, albeit at 10-fold higher concentration. PLA2G4E and PLAATs bear no structural or sequence similarities and belong to different protein classes (serine and cysteine hydrolases, respectively), but they have similar biosynthetic activity. This suggests that the active sites of these two enzyme families have evolved in convergent evolutionary pathways to recognize similar phospholipids as substrates. This may potentially explain why both NAPE-producing enzyme families also interact with **WEN091**. In line, **WEN091** inhibited phospholipase PLAAT3 less effectively than principal acyltransferases PLAAT2, PLAAT4 and PLAAT5.[18] Previously, selective PLAAT inhibitors that do not cross-react with PLA2G4E were reported.[44,50] Combining this tool set with **WEN091** may allow to investigate the activity of PLA2G4E and NAPEs in various tissues under normal and pathological conditions (e.g. ischemia or inflammation).[17,39] This will increase the understanding of the (patho)physiological role of PLA2G4E, PLAATs and their products, which may provide new therapeutic opportunities.[8,40,51]

Overexpression of PLA2G4E in Neuro-2a cells resulted in elevated levels of NAPEs, lyso-NAPEs, GP-NAEs and NAEs, which confirms that the formation of the (lyso)-NAPEs by PLA2G4E is the rate-limiting step in biosynthetic pathways of these signaling lipids. In line with previous findings[6], PLA2G4E overexpression resulted in increased levels of all NAPE species analyzed. The greater increase in *N*-16:0 and *N*-18:1 species reflects the relative abundance of these lipid chains in PC, suggesting limited substrate preference of PLA2G4E.[52] Treatment with control compound **WEN258** increased the levels of some NAPEs, which could be the result of inhibition of NAPE-metabolizing enzymes (e.g. ABHD4 or FAAH). As **WEN091** and **WEN258** share a similar off-target profile, this could indicate that the effect of **WEN091** on NAPE levels is underestimated due to inhibition of other enzymes.

The elevated levels of lyso-NAPEs and GP-PEA in PLA2G4E-overexpressing cells could be the result of ABHD4 activity in these cells, which has been reported before.[53] Treatment with **WEN091** or **WEN258** decreased GP-PEA levels, indicating both compounds inhibited ABHD4, which is in line with **WEN091**'s chemical proteomics results (Supplementary Figure S3.3). In contrast, lyso-NAPE levels were in general lowered by **WEN091**, but not affected by **WEN258**. This suggests the existence of an ABHD4-independent biosynthesis pathway for these lipids. Previously, Ca^{2+}-dependent *N*-acylation of lyso-PE in ischemic tissue has been suggested.[54] This activity might be attributed to PLA2G4E, leading to the hypothesis that PLA2G4E is responsible for the direct biosynthesis of both NAPEs and lyso-NAPEs in these cells (Figure 3.8). *N*-22:6 NAPE levels were elevated by PLA2G4E overexpression, but *N*-22:6 lyso-NAPEs were not. Treatment with **WEN091** or **WEN258** increased *N*-22:6 lyso-NAPE levels, possibly through inhibition of their degradation by ABHD4. This might suggest that these specific species are biosynthesized in a PLA2G4E-independent manner. Further research is needed to dissect the specific metabolic pathways of the individual lipid species. Both **WEN091** and **WEN258** lowered the levels of 2-AG and FFAs. The cABPP results showed that **WEN091** inhibited 2-AG-producing enzyme DAGLβ, but **WEN258** did not. Both compounds, however, inhibited ABHD6, which was previously reported to have diacylglycerol lipase activity in Neuro-2a (see also Chapter 6).[53] Thus, these results may indicate that ABHD6 is responsible for tonic 2-AG levels in these cells. As many enzymes are involved in FFA production (including PLA2G4A, ABHD4, ABHD6 and FAAH), inhibition of one or more of these enzymes by both compounds can account for the observed changes.

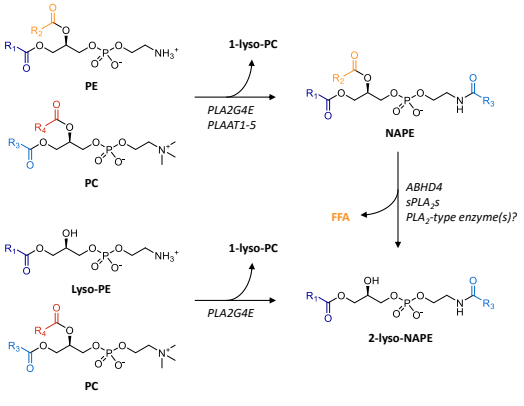

Figure 3.8. Putative updated overview of lyso-NAPE biosynthesis pathways. This work suggests the existence of ABHD4-independent NAPE-hydrolytic activity, which could be attributed to secretory PLA_2s ($sPLA_2$s) or other unidentified PLA_2-type enzymes, or to direct biosynthesis of lyso-NAPEs from lyso-PE by PLA2G4E. R = saturated, mono- or polyunsaturated fatty acyl.

Triazole urea-based inhibitors have been leveraged for targeting multiple enzymes within the serine hydrolase superfamily, including ABHD6, DAGLα, DDHD2 and LyPLA1/2.[47,55–58] The cellular selectivity of azole urea-based inhibitors was previously shown to deviate from the biochemical profile[49,59], as was observed with **WEN091** in this study. Tuning the reactivity of the urea and the interactions of the azole with the active site is likely important to obtain selectivity.[60] Further improvement of the selectivity profile of **WEN091** using these parameters is required to investigate the effects of acute PLA2G4E inhibition in cellular and *in vivo* systems (see Chapter 4).

Acknowledgements

Michael Schafroth and Benjamin Cravatt are kindly acknowledged for performing NAT assays and chemical proteomics, Xinyu Di, Thomas Hankemeier and Wouter Driever for targeted lipidomics, Wouter Driever and Laura de Paus for selectivity assays. Hans den Dulk and Tom van der Wel are acknowledged for plasmid cloning and purification.

Experimental procedures

General remarks

All reagents and chemicals were obtained from Bio-Rad or Thermo Fisher Scientific, solvents from Sigma-Aldrich and used without further purification, unless otherwise noted. Activity-based probes were purchased from Thermo Fisher Scientific (FP-TAMRA) or synthesized in-house (MB064)[61] (Chemical structures shown in Supplementary Figure S3.8). **WEN091** was synthesized as described in Chapter 2.

Plasmids

The full-length cDNA of wild type human PLA2G4E (GenScript Biotech), murine PLA2G4B, hPLA2G4C, mPLA2G4D (Source BioScience), hPLAAT2–5 and hNAPE-PLD (kindly provided by Prof. Natsuo Ueda) were cloned into pcDNA™3.1(+) expression vectors in-frame with a C-terminal FLAG tag. Plasmids were isolated from transformed *Escherichia coli* XL-10 using a Qiagen Plasmid Midi kit and stored at 4°C in TE buffer (10 mM Tris, 0.1 mM EDTA, pH 8.0). The sequence was determined (Macrogen) and verified using CLC Main Workbench.

Cell culture

HEK293T (human embryonic kidney) and Neuro-2a (murine neuroblastoma) cells (ATCC) were cultured in Dulbecco's Modified Eagle's Medium (DMEM, Sigma-Aldrich D6546) with additional heat-inactivated newborn calf serum (10% (v/v), Avantor Seradigm), L-Ala-L-Gln (2 mM, Sigma-Aldrich), penicillin and streptomycin (both 200 µg/mL, Duchefa Biochemie) at 37°C, 7% CO_2. Medium was refreshed every 2–3 days and cells were passaged twice a week at 70–80% confluence by aspirating the medium, thorough pipetting in fresh medium and seeding to appropriate density. Cell cultures were regularly tested for mycoplasma and discarded after 2–3 months.

Overexpression lysate preparation

One day prior to transfection, 10^7 HEK293T cells were seeded to a 15 cm dish. For transfection, medium was replaced with 13 mL fresh medium. Per 15 cm dish, 20 µg pcDNA™3.1(+) plasmid was dissolved in 1 mL serum-free DMEM and mixed with 1 mL serum-free DMEM containing 60 µg polyethyleneimine (PEI, Polysciences). The mixture was incubated for 15 min and added dropwise to the cells. 24 h p.t., medium was replaced with 25 mL fresh medium. 72 h p.t., medium was aspirated, cells were washed with Dulbecco's PBS (DPBS, Sigma-Aldrich D8537, RT) and harvested in DPBS (RT) by thorough pipetting. Cells were centrifuged (3000 × *g*, 15 min), pellets were flash-frozen in liquid N_2 and stored at −80°C until further use.

Cell pellets were thawed on ice, homogenized in 2 mL ice-cold lysis buffer (50 mM Tris-HCl, 2 mM DTT, 1 mM $MgCl_2$, 5 U/mL Benzonase® (Santa Cruz Biotechnology, Inc.), pH 8.0 with additional 3 mM $CaCl_2$ for hPLA2G4E) per 15 cm cell culture dish using a Sonics® Vibra-Cell VCX 130 probe sonicator equipped with a 2 mm microtip (3 × 10 s on/10 s off, 20% amplitude). After incubation on ice for 30 min, the insoluble ("membrane") fraction was separated from the soluble ("cytosol") fraction by ultracentrifugation (10^5 × *g*, 35 min, 4°C, Beckman-Coulter ultracentrifuge, Ti70.1 rotor). The pellet was resuspended in 1 mL ice-cold storage buffer (50 mM Tris-HCl, 2 mM DTT, pH 8.0 with additional 3 mM $CaCl_2$ for hPLA2G4E) per 15 cm plate and homogenized by passing through an insulin needle. After determination of the protein concentration using a Quick Start™ Bradford Protein Assay, the samples were diluted to 1.0 mg/mL (hPLA2G4E, mPLA2G4B, hPLA2G4C and mPLA2G4D) or 0.5 mg/mL (mPLA2G4E) in ice-cold storage buffer, aliquoted to single-use volumes, flash-frozen in liquid N_2 and stored at −80°C until use.

mPLA2G4E plasmids were cloned as described before[6]. 48 h p.t., medium was aspirated, cells were washed with PBS and harvested by scraping in PBS. After centrifugation the pellet was resuspended in lysis buffer (50 mM Tris-HCl, 0.5% IGEPAL CA-630, pH 8.0) and sonicated. Insoluble proteins were removed by ultracentrifugation ($10^5 \times g$, 15 min), after which the supernatant was aliquoted, flash-frozen in liquid N_2 and stored at −80°C until use.

hPLAAT2–5, hNAPE-PLD and $CB_{1/2}$ overexpression and lysate preparation was performed as described before.[44,46]

Mouse brain lysate preparation

For ABPP experiments, mouse brains were harvested from surplus C57Bl/6J mice (8–14 weeks old) that were killed by cervical dislocation, according to guidelines approved by the ethical committee of Leiden University (AVD1060020171144), immediately flash-frozen in liquid N_2 and stored at −80°C until use. Upon preparation, intact brains were thawed on ice and homogenized in 6 mL ice-cold lysis buffer (20 mM HEPES, 2 mM DTT, 250 mM sucrose, 1 mM $MgCl_2$, 25 U/mL Benzonase®, pH 6.8) using a Wheaton™ dounce homogenizer (DWK Life Sciences) and incubated on ice for 1 h. Cell debris was removed by low-speed centrifugation (170 × *g*, 5 min, 4°C), after which the supernatant was subjected to ultracentrifugation to separate insoluble ("membrane") and soluble ("cytosol") fractions ($10^5 \times g$, 35 min, 4°C, Beckman-Coulter ultracentrifuge, Ti70.1 rotor). The pellet was resuspended in ice-cold storage buffer (20 mM HEPES, 2 mM DTT, pH 6.8) and homogenized by passing through an insulin needle. The protein concentrations of both fractions were determined using a Quick Start™ Bradford Protein Assay and samples were diluted to 2.0 mg/mL (membrane) or 1.0 mg/mL (cytosol) using ice-cold storage buffer, aliquoted to single-use volumes, flash-frozen in liquid N_2 and stored at −80°C until use.

For Ca-NAT activity assays, mouse brains were harvested from male C57Bl/6J mice (10 weeks old) which were anesthetized with isoflurane and killed by cervical dislocation, according to guidelines approved by The Scripps Research Institute-Institutional Animal Care and Use Committee Office, immediately flash-frozen in liquid N_2 and stored at −80°C until use. Upon preparation, intact brains were thawed on ice and homogenized in 5 volumes (v/w) ice-cold lysis buffer (50 mM Tris-HCl, 320 mM sucrose, pH 8.0) using a dounce homogenizer. Ultracentrifugation ($10^5 \times g$, 15 min) yielded the cytosol fraction as supernatant, after which the pellet was washed with 50 mM Tris-HCl, 1 M NaCl (pH 8.0) and centrifuged again. The resulting pellet was resuspended in 50 mM Tris-HCl (pH 8.0) and used as membrane fraction. Fractions were aliquoted, flash-frozen in liquid N_2 and stored at −80°C until use.

Activity-based protein profiling

HEK293T or mouse brain lysates were thawed on ice. 19.5 µL lysate was incubated with 0.5 µL inhibitor solution in DMSO (Sigma-Aldrich) for 30 min (RT), followed by addition of 0.5 µL probe in DMSO (hPLA2G4E: FP-TAMRA, 50 nM, 5 min; mPLA2G4E: FP-TAMRA, 100 nM, 5 min; mPLA2G4B, hPLA2G4C, mPLA2G4D: FP-TAMRA, 500 nM, 20 min; hPLAAT2, hPLAAT3: MB064, 250 nM, 20 min; hPLAAT4, hPLAAT5: MB064, 500 nM, 20 min; mouse brain: FP-TAMRA, 500 nM, 20 min or MB064, 250 nM, 20 min, RT. Final DMSO concentration 5% (v/v)). The reaction was quenched by addition of 7 µL 4× Laemmli sample buffer (240 mM Tris, 8% (w/v) SDS, 40% (v/v) glycerol, 5% (v/v) β-mercaptoethanol (Sigma-Aldrich), 0.04% bromophenol blue) and incubation for 15 min at RT. 10 µL sample was resolved on 8% (hPLA2G4E), 10% (mPLA2G4E, mPLA2G4B, hPLA2G4C, mPLA2G4D, mouse brain) or 15% (hPLAAT2–5) acrylamide SDS-PAGE gels (180V, 75 min) and the gel was imaged on a Bio-Rad Chemidoc MP using Cy3/TAMRA settings (ex. 532/12 nm, em. 602/50 nm). Coomassie Brilliant Blue

R250 staining was used for total protein loading correction. Images were analyzed using Bio-Rad Image Lab 6. IC_{50} calculations were performed in GraphPad Prism 7.

In vitro NAPE production assay

HEK293T overexpression lysate (diluted to 40 µL 0.1 mg/mL in assay buffer (50 mM Tris-HCl, 2 mM DTT, 3 mM $CaCl_2$, 0.1% IGEPAL CA-630, pH 8.0)) or mouse brain membrane proteome (diluted to 40 µL 2.0 mg/mL in assay buffer) were incubated with inhibitor in DMSO (30 min, 37°C), followed by treatment with *sn*-1,2-dipalmitoylphosphatidylcholine (DPPC, Avanti Polar Lipids) and *sn*-1,2-dioleoylphosphatidylethanolamine (DOPE, Cayman Chemicals) (final concentrations 40 µM and 75 µM, respectively (HEK293T), or 250 µM each (mouse brain)) for 30 (HEK293T) or 60 min (mouse brain) at 37°C. Reactions were quenched by addition of 150 µL 2:1 MeOH:$CHCl_3$ containing 10 pmol *N*-C19:1 DOPE internal standard[23], followed by 50 µL $CHCl_3$ and 50 µL 0.9% KCl in water. After centrifugation, layers were separated and 100 µL of the organic layer was mixed with 50 µL MeOH.

The sample was injected into the LC-MS system consisting of an LC/MSD (Agilent Technologies). Separation was performed in a Phenomenex Gemini C18 analytical column (50 mm × 4.6 mm × 5 µm) coupled to a Gemini C18 guard column (4 × 3 mm). The mobile phase consisted of 14 mM NH_4OH in 95:5 (v/v) H_2O:MeOH (A) and 14 mM NH_4OH in 60:35:5 *i*PrOH:MeOH:H_2O (B). The elution method started with 0.1 mL/min 90% A for 5 min, followed by 0.4 mL 100% B for 6.5 min and final equilibration with 0.5 mL/min 90% A for 2 min. Lipids were detected with electrospray ionization (ESI) operating in negative ion mode and MS acquisition in selected ion monitoring mode (m/z 980.8 and 1020.8 for *N*-C16:0 DOPE product and *N*-C19:1 DOPE internal standard, respectively).

NAPE-PLD activity assay

The activity of hNAPE-PLD was measured in a fluorogenic surrogate substrate assay based on *N*-((6-(2,4-dinitrophenyl)amino)hexanoyl)-2-(4,4-difluoro-5,7-dimethyl-4-bora-3a,4a-diaza-*s*-indacene-3-pentanoyl)-1-hexadecanoyl-*sn*-glycero-3-phosphoethanolamine, triethylammonium salt (PED6) as described before, with minor alterations.[45] Fluorescence measurements were performed in a BMG LABTECH CLARIOstar® plate reader, scanning every 2 minutes for 1 h (37°C, ex. 485 nm, em. 535 nm, gain 1054). The slope of t = 2 min to t = 6 min was used as the enzymatic rate (RFU/min), which was normalized to generate IC_{50} curves in GraphPad Prism 9. All measurements were performed in N = 2, n = 2 or N = 2, n = 4 for controls and only accepted when Z' ≥ 0.6.

$CB_{1/2}$ assay

The [^{3}H]CP55,940 displacement assay was performed as described before.[46]

Chemical proteomics

Sample preparation

Mouse brain membrane or cytosol proteome (500 µL, 2.0 mg/mL in 50 mM Tris-HCl, 2 mM DTT, 3 mM $CaCl_2$, pH 8.0) was incubated with DMSO or 1 µM WEN091 in DMSO for 30 min (37°C), followed by labeling of residual enzyme activity with 4 µM FP-biotin for 60 min (RT). Labeling of heat-denatured proteome was used as control. Reactions were quenched by protein precipitation in 2.5 mL 4:1 MeOH/$CHCl_3$. The mixture was centrifuged (5000 × *g*, 15 min, 4°C), after which the pellet was washed with 1:1 MeOH/$CHCl_3$ (3 × 1 mL) and then probe sonicated in 2.5 mL 4:1 MeOH/$CHCl_3$ and pelleted again (5000 × *g*, 15 min, 4°C). The pellet was redissolved in 500 µL 50 mM Tris-HCl, 6 M urea, 2% (w/v) SDS, 10 mM DTT, pH 8.0, reduced using Tris(2-carboxyethyl)phosphine (TCEP) (10 mM, 30 min, 37°C) and methylated with iodoacetamide (20 mM, 30 min, 25°C in the dark). Biotinylated proteins were enriched by sequential addition of 140 µL 10% (w/v) SDS, 5.5 mL PBS and 20 µL PBS-washed avidin-

agarose beads (Sigma-Aldrich) and shaking (1.5 h, 25°C). Beads were pelleted (1000 × *g*, 2 min), washed sequentially with 0.2% (w/v) SDS in PBS (3 × 10 mL), PBS (3 × 10 mL) and 100 mM triethylammonium bicarbonate (3 × 10 mL) and transferred to an Eppendorf LoBind® tube. On-bead digestion was performed using Promega Sequencing Grade trypsin (500 ng) in 100 mM triethylammonium bicarbonate. Resulting peptides were labeled with either 4% formaldehyde ("light") or ^{13}C-labeled deuterated formaldehyde ("heavy") (0.15% final concentration) in combination with $NaBH_3CN$ (22.2 mM, 1h, RT). The reaction was quenched by addition of 1% NH_4OH and 5% formic acid (final concentrations 0.23% and 0.5%, respectively), after which the light and heavy-labeled samples were combined for analysis.

LC-MS/MS analysis

4 µL was injected into the LC-MS/MS system, consisting of an Agilent 1200 HPLC coupled to an LTQ Orbitrap Velos. Separation was performed on an in-house packed tip column (Phenomenex Gemini 5 µm C18, 150 × 0.1 mm), using a linear gradient of CH_3CN in 0.1% formic acid with a flow rate of 300 nL/min. Each full-scan mass spectrum (350–2000 *m/z*) was followed by top 20 data-dependent MS/MS scans. Dynamic exclusion was used with an exclusion list of 500 and a repeat time of 20 s.

MS/MS spectra were searched against a FASTA file of serine hydrolases assembled from the mouse UniProt database (retrieved Nov 9, 2012) with the ProLuCID algorithm using a target-decoy approach, in which each protein sequence was reversed and concatenated to the normal database. Search parameters were set to a 50-ppm precursor mass tolerance, with carbamidomethylation of cysteine residues (+57.0215 Da) as a static modification and oxidation of methionine residues (+15.9949 Da) as a variable modification. In addition, methylation of lysine residues and N-termini (light: +28.0313 Da, heavy: +34.06312 Da) was specified as static modification. Search results were filtered with DTASelect 2.0.47, limiting to tryptic peptides and applying a peptide FDR < 1%, and for serine hydrolase annotations (both reviewed and unreviewed). Ratios of peak areas were quantified using CIMAGE software by generating a MS1 chromatogram (± 10 ppm) using a retention time window of ± 10 min centered on the time the peptide was selected for fragmentation. Computation filters included a co-elution correlation score $R^2 \geq 0.8$ and an isotopic envelope correlation score $R^2 > 0.8$. Proteins only detected in either light or heavy-labeled samples were manually given a maximal or minimal ratio of 5 or 0.05, respectively.

Cellular ABPP assay

Two days prior to the experiment, Neuro-2a cells were seeded to 12-wells plates (~$0.25 \cdot 10^6$ cells per well). Before the experiment was started, medium was aspirated. Medium with DMSO or inhibitor in DMSO (0.25% (v/v) DMSO) was added and cells were incubated for 30 min at 37°C. Then medium was aspirated and cells were washed with DPBS (RT). Cells were harvested in ice-cold DPBS by thorough pipetting and centrifuged (1000 × *g*, 6 min, RT). Pellets were flash-frozen in liquid N_2 and stored at −80°C until further use.

Cell pellets were thawed on ice and lysed in 50 µL lysis buffer (20 mM HEPES, 2 mM DTT, 250 mM sucrose, 1 mM $MgCl_2$, 25 U/mL Benzonase®, pH 6.8). After incubation on ice for 20 min, the protein concentration was determined using Quick Start™ Bradford Protein Assay and the samples were diluted to 2.0 mg/mL using storage buffer (20 mM HEPES, 2 mM DTT, pH 6.8). 19.5 µL of this whole lysate was incubated with FP-TAMRA (500 nM) or MB064 (2 µM) in DMSO (20 min, RT). Reactions were then quenched with 7 µL 4× Laemmli sample buffer and proteins were resolved and images analyzed as described under Activity-based protein profiling.

Targeted lipidomics

Sample preparation

One day prior to transfection, Neuro-2a cells were seeded to 6-cm dishes (~$1.8 \cdot 10^6$ cells per dish). Upon transfection, medium was replaced with 2 mL fresh medium. Per dish, 1 µg PLA2G4E or mock plasmid was dissolved in 100 µL serum-free DMEM and mixed with 100 µL serum-free DMEM containing 5 µg polyethyleneimine (PEI, Polysciences). The mixture was incubated for 15 min and added dropwise to the cells. After 24 h, cells were harvested or inhibitor treatment was started. For harvest, medium was removed and cells were washed with 500 µL DPBS (RT) and harvested in 1250 µL DPBS by thorough pipetting. 1000 µL of the cell suspension was centrifuged (1000 × *g*, 5 min) in Eppendorf® Safe-Lock tubes and the pellet was flash-frozen in liquid N_2 and stored at −80°C until further use. The remaining 250 µL was used for cell count (Trypan Blue). For inhibitor experiments, inhibitor in DMSO was diluted in DMEM (0.25% (v/v) DMSO) to prepare treatment medium. Medium was replaced with 2 mL treatment medium per dish and cells were incubated for 8 h (37°C). Cells were harvested as described above.

Lipid extraction

Pellets were thawed on ice. To each sample 10 µL internal standard mix (reference lipids *N*-heptadecanoyl (17:0)-1,2-dioleoyl (18:1)-*sn*-glycero-3-phosphoethanolamine, *N*-heptadecanoyl-1-oleoyl-2-lyso-*sn*-glycero-3-phosphoethanolamine, *N*-heptadecanoyl-1-(1-enyl-stearoyl) (p18:0)-2-stearoyl (18:0)-*sn*-glycero-3-phosphoethanolamine, *N*-heptadecanoyl-1-(1-enyl-stearoyl)-2-lyso-*sn*-glycero-3-phosphoethanolamine (all synthesized in-house), *N*-palmitoyl (16:0) ethanolamine-d_4, *N*-stearoyl ethanolamine-d_3, *N*-oleoyl ethanolamine-d_4, *N*-linoleoyl (18:2) ethanolamine-d_4, *N*-arachidonoyl (20:4) ethanolamine-d_8, *N*-docosahexaenoyl (22:6) ethanolamine-d_4 and 2-arachidonoylglycerol-d_8 (Cayman Chemical Company)) was added, followed by 100 µL extraction buffer (0.2 M citric acid, 0.1 M Na_2HPO_4, pH 4) and 1000 µL extractant (1:1 (v/v) MTBE:BuOH). Samples were mixed in a Next Advance Bullet Blender® Blue tissue homogenizer (5 min, 90% speed, RT) and centrifuged (16,000 × *g*, 10 min, 4°C). 950 µL of the organic layer was transferred to clean, pre-cooled tubes and concentrated in a SpeedVac Vacuum Concentrator (Thermo Fisher Scientific). 50 µL reconstitution solution (1:1 (v/v) BuOH:CH_3CN) was added and the samples were agitated for 15 min, after which they were centrifuged (16,000 × *g*, 10 min, 4°C). 40 µL was transferred into autosampler vials with inserts. Samples were kept at 7°C in the autosampler for less than 24 h before analysis. Quality control (QC) samples were simultaneously prepared using blank cell pellets.

LC-MS/MS analysis

10 µL of sample was analyzed using a Shimadzu LC system hyphenated with a SCIEX QTRAP® 6500+ mass spectrometer. Separation was performed on a Acquity BEH C8 column (2.1 × 50 mm, 1.7 µm) (Waters Corporation) maintained at 40°C, with the eluent flow rate set to 0.4 mL/min. The mobile phase consisted of 2 mM NH_4HCO_2, 10 mM formic acid in water (A), CH_3CN (B) and isopropanol (C). Initial gradient conditions were 20% B, 20% C for 1 min, followed by linear increase to 40% B, 20% C over the course of 1 min, which was held for 5 min. It was then linearly increased to 40% B, 50% C over the course of 1 min, which was held for 2.5 min. The system returned to initial conditions and was re-equilibrated for 1.5 min. Electrospray ionization (ESI)-MS acquisition was carried out in positive and negative mode with the following ESI parameters: source temperature: 600°C, nebulizer gas: 50 L/min, heater gas: 50 L/min, curtain gas: 30 L/min, collision gas: medium, ion spray voltage: ±4500 V. Selected reaction monitoring (SRM) was used for data acquisition. Peak detection and integration were carried out in SCIEX OS software. Relative lipid levels were calculated as the ratio of analyte peak

to corresponding internal standard. QC samples were regularly injected during the measurements to evaluate the quality of the data, including blank effect (BE), retention time shifts and relative standard deviation (RSD) calculated for analyte present in the QC samples. Metabolites with BE ≤ 40% and RSD ≤ 30% were included for further analysis. Metabolites with 15% ≤ RSD ≤ 30% were reported, but should be interpreted with caution. Relative lipid levels were corrected for cell count and normalized to mock-transfected cells or DMSO-treated cells. Relative levels were transferred to GraphPad Prism 8 for statistical analysis. Each lipid was tested for equality between treatment and control groups using one-way ANOVA with Dunnett's multiple comparison correction.

References

1. Leslie, C. C. Cytosolic phospholipase A_2: Physiological function and role in disease. *J. Lipid Res.* **56**, 1386–1402 (2015).
2. Murakami, M. *et al.* Recent progress in phospholipase A_2 research: From cells to animals to humans. *Prog. Lipid Res.* **50**, 152–192 (2011).
3. Ghomashchi, F. *et al.* Interfacial kinetic and binding properties of mammalian group IVB phospholipase A_2 (cPLA$_2$β) and comparison with the other cPLA$_2$ isoforms. *J. Biol. Chem.* **285**, 36100–36111 (2010).
4. Ohto, T., Uozumi, N., Hirabayashi, T. & Shimizu, T. Identification of novel cytosolic phospholipase A$_2$s, murine cPLA$_2$δ, ε, and ζ, which form a gene cluster with cPLA$_2$β. *J. Biol. Chem.* **280**, 24576–24583 (2005).
5. Ghosh, M., Tucker, D. E., Burchett, S. A. & Leslie, C. C. Properties of the Group IV phospholipase A_2 family. *Prog. Lipid Res.* **45**, 487–510 (2006).
6. Ogura, Y., Parsons, W. H., Kamat, S. S. & Cravatt, B. F. A calcium-dependent acyltransferase that produces *N*-Acyl phosphatidylethanolamines. *Nat. Chem. Biol.* **12**, 669–671 (2016).
7. Hussain, Z. *et al.* Phosphatidylserine-stimulated production of *N*-acyl-phosphatidylethanolamines by Ca^{2+}-dependent *N*-acyltransferase. *Biochim. Biophys. Acta - Mol. Cell Biol. Lipids* **1863**, 493–502 (2018).
8. Wellner, N., Diep, T. A., Janfelt, C. & Hansen, H. S. *N*-acylation of phosphatidylethanolamine and its biological functions in mammals. *Biochim. Biophys. Acta - Mol. Cell Biol. Lipids* **1831**, 652–662 (2013).
9. Hansen, H. S., Moesgaard, B., Hansen, H. H., Schousboe, A. & Petersen, G. Formation of *N*-acyl-phosphatidylethanolamine and *N*-acylethanolamine (including anandamide) during glutamate-induced neurotoxicity. *Lipids* **34**, S327–S330 (1999).
10. Swamy, M. J., Tarafdar, P. K. & Kamlekar, R. K. Structure, phase behaviour and membrane interactions of *N*-acylethanolamines and *N*-acylphosphatidylethanolamines. *Chem. Phys. Lipids* **163**, 266–279 (2010).
11. Térová, B., Petersen, G., Hansen, H. S. & Slotte, J. P. *N*-acyl phosphatidylethanolamines affect the lateral distribution of cholesterol in membranes. *Biochim. Biophys. Acta - Biomembr.* **1715**, 49–56 (2005).
12. Shangguan, T., Pak, C. C., Ali, S., Janoff, A. S. & Meers, P. Cation-dependent fusogenicity of an *N*-acyl phosphatidylethanolamine. *Biochim. Biophys. Acta* **1368**, 171–183 (1998).
13. Palese, F., Pontis, S., Realini, N. & Piomelli, D. NAPE-specific phospholipase D regulates LRRK2 association with neuronal membranes. in *Advances in Pharmacology* **90**, 217–238 (Academic Press Inc., 2021).
14. Mileykovskaya, E. & Dowhan, W. Role of membrane lipids in bacterial division-site selection. *Curr. Opin. Microbiol.* **8**, 135–142 (2005).
15. Gillum, M. P. *et al. N*-acylphosphatidylethanolamine, a Gut-Derived Circulating Factor Induced by Fat Ingestion, Inhibits Food Intake. *Cell* **135**, 813–824 (2008).
16. Romano, A., Tempesta, B., Provensi, G., Passani, M. B. & Gaetani, S. Central mechanisms mediating the hypophagic effects of oleoylethanolamide and *N*-acylphosphatidylethanolamines: Different lipid signals? *Front. Pharmacol.* **6**, 1–8 (2015).
17. Shiratsuchi, A. *et al.* Inhibitory effect of *N*-palmitoylphosphatidylethanolamine on macrophage phagocytosis through inhibition of Rac1 and Cdc42. *J. Biochem.* **145**, 43–50 (2008).

18. Uyama, T. *et al.* Generation of *N*-acylphosphatidylethanolamine by members of the phospholipase A/acyltransferase (PLA/AT) family. *J. Biol. Chem.* **287**, 31905–31919 (2012).
19. Uyama, T., Jin, X. H., Tsuboi, K., Tonai, T. & Ueda, N. Characterization of the human tumor suppressors TIG3 and HRASLS2 as phospholipid-metabolizing enzymes. *Biochim. Biophys. Acta - Mol. Cell Biol. Lipids* **1791**, 1114–1124 (2009).
20. Okamoto, Y., Morishita, J., Tsuboi, K., Tonai, T. & Ueda, N. Molecular Characterization of a Phospholipase D Generating Anandamide and Its Congeners. *J. Biol. Chem.* **279**, 5298–5305 (2004).
21. Tsuboi, K. *et al.* Glycerophosphodiesterase GDE4 as a novel lysophospholipase D: A possible involvement in bioactive *N*-acylethanolamine biosynthesis. *Biochim. Biophys. Acta - Mol. Cell Biol. Lipids* **1851**, 537–548 (2015).
22. Sun, Y. X. *et al.* Biosynthesis of anandamide and *N*-palmitoylethanolamine by sequential actions of phospholipase A2 and lysophospholipase D. *Biochem. J.* **380**, 749–756 (2004).
23. Simon, G. M. & Cravatt, B. F. Endocannabinoid biosynthesis proceeding through glycero-phospho-*N*-acyl ethanolamine and a role for α/β-hydrolase 4 in this pathway. *J. Biol. Chem.* **281**, 26465–26472 (2006).
24. Liu, J. *et al.* Multiple pathways involved in the biosynthesis of anandamide. *Neuropharmacology* **54**, 1–7 (2008).
25. Rahman, I. A. S. *et al.* Calcium-dependent generation of *N*-acylethanolamines and lyso-phosphatidic acids by glycerophosphodiesterase GDE7. *Biochim. Biophys. Acta - Mol. Cell Biol. Lipids* **1861**, 1881–1892 (2016).
26. Simon, G. M. & Cravatt, B. F. Anandamide biosynthesis catalyzed by the phosphodiesterase GDE1 and detection of glycerophospho-*N*-acyl ethanolamine precursors in mouse brain. *J. Biol. Chem.* **283**, 9341–9349 (2008).
27. Liu, J. *et al.* A biosynthetic pathway for anandamide. *Proc. Natl. Acad. Sci. U. S. A.* **103**, 13345–13350 (2006).
28. Mattace Raso, G., Russo, R., Calignano, A. & Meli, R. Palmitoylethanolamide in CNS health and disease. *Pharmacol. Res.* **86**, 32–41 (2014).
29. Petrosino, S. & Di Marzo, V. The pharmacology of palmitoylethanolamide and first data on the therapeutic efficacy of some of its new formulations. *Br. J. Pharmacol.* **174**, 1349–1365 (2017).
30. Dalle Carbonare, M. *et al.* A saturated *N*-acylethanolamine other than *N*-palmitoyl ethanolamine with anti-inflammatory properties: A neglected story... *J. Neuroendocrinol.* **20**, 26–34 (2008).
31. Fu, J. *et al.* Oleylethanolamide regulates feeding and body weight through activation of the nuclear receptor PPAR-α. *Nature* **425**, 90–93 (2003).
32. Tsuboi, K., Uyama, T., Okamoto, Y. & Ueda, N. Endocannabinoids and related *N*-acylethanol-amines: biological activities and metabolism. *Inflamm. Regen.* **38**, (2018).
33. Morena, M. *et al.* Upregulation of anandamide hydrolysis in the basolateral complex of amygdala reduces fear memory expression and indices of stress and anxiety. *J. Neurosci.* **39**, 1275–1292 (2019).
34. Devane, W. A. *et al.* Isolation and structure of a brain constituent that binds to the cannabinoid receptor. *Science* **258**, 1946–1949 (1992).
35. Maccarrone, M. *et al.* Anandamide inhibits metabolism and physiological actions of 2-arachidonoylglycerol in the striatum. *Nat. Neurosci.* **11**, 152–159 (2008).
36. Katona, I. & Freund, T. F. Multiple Functions of Endocannabinoid Signaling in the Brain. *Annu. Rev. Neurosci.* **35**, 529–558 (2012).

37. Fotio, Y., Ciccocioppo, R. & Piomelli, D. *N*-acylethanolamine acid amidase (NAAA) inhibition decreases the motivation for alcohol in Marchigian Sardinian alcohol-preferring rats. *Psychopharmacology* **238**, 249–258 (2021).
38. Cravatt, B. F. *et al.* Molecular characterization of an enzyme that degrades neuromodulatory fatty-acid amides. *Nature* **384**, 83–87 (1996).
39. Berger, C. *et al.* Massive accumulation of *N*-acylethanolamines after stroke. Cell signalling in acute cerebral ischemia? *J. Neurochem.* **88**, 1159–1167 (2004).
40. Palese, F., Pontis, S., Realini, N. & Piomelli, D. A protective role for *N*-acylphosphatidylethanol-amine phospholipase D in 6-OHDA-induced neurodegeneration. *Sci. Rep.* **9**, 1–16 (2019).
41. Tuo, W. *et al.* Therapeutic Potential of Fatty Acid Amide Hydrolase, Monoacylglycerol Lipase, and *N*-Acylethanolamine Acid Amidase Inhibitors. *J. Med. Chem.* **60**, 4–46 (2016).
42. Cadas, H., Di Tomaso, E. & Piomelli, D. Occurrence and biosynthesis of endogenous cannabinoid precursor, *N*-arachidonoyl phosphatidylethanolamine, in rat brain. *J. Neurosci.* **17**, 1226–1242 (1997).
43. Mock, E. D. *et al.* Discovery of a NAPE-PLD inhibitor that modulates emotional behavior in mice. *Nat. Chem. Biol.* **16**, 667–675 (2020).
44. Zhou, J. *et al.* Structure-Activity Relationship Studies of α-Ketoamides as Inhibitors of the Phospholipase A and Acyltransferase Enzyme Family. *J. Med. Chem.* **63**, 9340–9359 (2020).
45. Mock, E. D. *et al.* Structure-Activity Relationship Studies of Pyrimidine-4-Carboxamides as Inhibitors of *N*-Acylphosphatidylethanolamine Phospholipase D. *J. Med. Chem.* **64**, 481–515 (2021).
46. Soethoudt, M. *et al.* Cannabinoid CB_2 receptor ligand profiling reveals biased signalling and off-target activity. *Nat. Commun.* **8**, (2017).
47. Hsu, K. L. *et al.* Discovery and optimization of piperidyl-1,2,3-triazole ureas as potent, selective, and *in vivo*-active inhibitors of α/β-hydrolase domain containing 6 (ABHD6). *J. Med. Chem.* **56**, 8270–8279 (2013).
48. Baggelaar, M. P. *et al.* Highly Selective, Reversible Inhibitor Identified by Comparative Chemoproteomics Modulates Diacylglycerol Lipase Activity in Neurons. *J. Am. Chem. Soc.* **137**, 8851–8857 (2015).
49. Janssen, A. P. A. Hit-to-Lead Optimization of Triazole Sulfonamide DAGL-α inhibitors. *Inhibitor Selectivity: Profiling and Prediction* (Leiden University, 2019).
50. Zhou, J. *et al.* Activity-Based Protein Profiling Identifies α-Ketoamides as Inhibitors for Phospholipase A2 Group XVI. *ACS Chem. Biol.* **14**, 164–169 (2019).
51. Coulon, D., Faure, L., Salmon, M., Wattelet, V. & Bessoule, J. J. Occurrence, biosynthesis and functions of *N*-acylphosphatidylethanolamines (NAPE): Not just precursors of *N*-acylethanolamines (NAE). *Biochimie* **94**, 75–85 (2012).
52. Sugiura, T. *et al.* Enzymatic synthesis of anandamide, an endogenous cannabinoid receptor ligand, through *N*-Acylphosphatidylethanolamine pathway in testis: Involvement of Ca^{2+}-dependent transacylase and phosphodiesterase activities. *Biochem. Biophys. Res. Commun.* **218**, 113–117 (1996).
53. van Esbroeck, A. C. M. *et al.* Identification of α,β-Hydrolase Domain Containing Protein 6 as a Diacylglycerol Lipase in Neuro-2a Cells. *Front. Mol. Neurosci.* **12**, (2019).
54. Natarajan, V., Reddy, P. V., Schmid, P. C. & Schmid, H. H. O. *N*-acylation of ethanolamine phospholipids in canine myocardium. *Biochim. Biophys. Acta - Lipids Lipid Metab.* **712**, 342–355 (1982).

55. Deng, H. *et al.* Triazole Ureas Act as Diacylglycerol Lipase Inhibitors and Prevent Fasting-Induced Refeeding. *J. Med. Chem.* **60**, 428–440 (2017).
56. Inloes, J. M. *et al.* The hereditary spastic paraplegia-related enzyme DDHD2 is a principal brain triglyceride lipase. *Proc. Natl. Acad. Sci. U. S. A.* **111**, 14924–14929 (2014).
57. Hulce, J. J. *et al.* An *in vivo* active carbamate-based dual inhibitor of Lysophospholipase 1 (LyPLA1) and Lysophospholipase 2 (LyPLA2). *Probe Reports From NIH Mol. Libr. Progr.* (2013).
58. Adibekian, A. *et al.* Click-generated triazole ureas as ultrapotent *in vivo*-active serine hydrolase inhibitors. *Nat. Chem. Biol.* **7**, 469–478 (2011).
59. Van Esbroeck, A. C. M. *et al.* Activity-based protein profiling reveals off-target proteins of the FAAH inhibitor BIA 10-2474. *Science* **356**, 1084–1087 (2017).
60. Janssen, A. P. A. *et al.* Structure Kinetics Relationships and Molecular Dynamics Show Crucial Role for Heterocycle Leaving Group in Irreversible Diacylglycerol Lipase Inhibitors. *J. Med. Chem.* **62**, 7910–7922 (2019).
61. Baggelaar, M. P. *et al.* Development of an activity-based probe and in silico design reveal highly selective inhibitors for diacylglycerol lipase-α in brain. *Angew. Chemie - Int. Ed.* **52**, 12081–12085 (2013).

Supplementary information

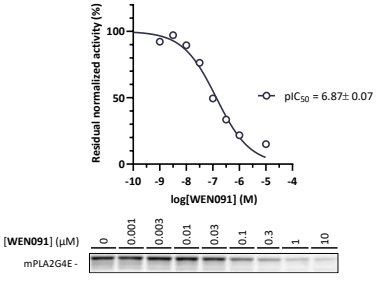

Supplementary Figure S3.1. Inhibition of mouse PLA2G4E by WEN091. Excerpt of cABPP gel on mPLA2G4E-overexpressing HEK293T lysate and corresponding inhibition curve and pIC_{50} value (preliminary, N = 1).

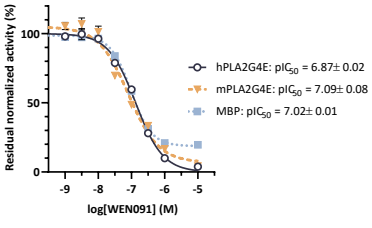

Supplementary Figure S3.2. Inhibition curves of WEN091 in NAPE production assay. Graph corresponding to Figure 3.2D–F. Curves generated from conversion rates of Ca-NAT activity assay on overexpression lysate and mouse brain proteome (MBP). Data presented as mean ± SEM (N = 2).

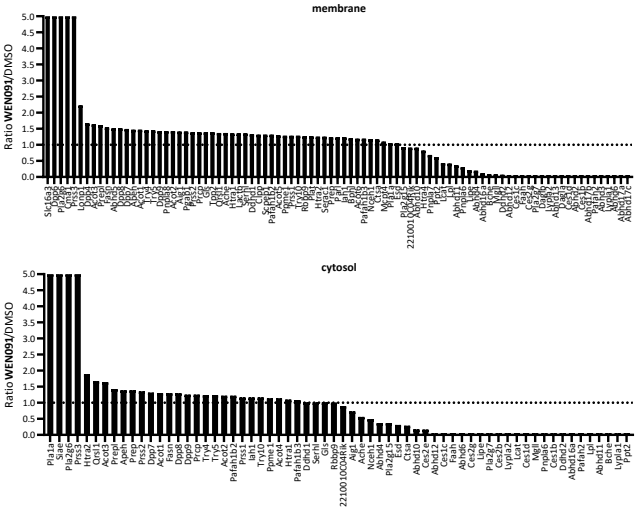

Supplementary Figure S3.3. Activity of WEN091 in chemical proteomics experiment. Mouse brain membrane or cytosol enzymes identified by LC-MS/MS in pulldown experiment with FP-biotin (4 μM, 60 min, RT) after pretreatment with **WEN091** (1 μM, 30 min, 37°C). Bars represent ratios of quantified peptides between **WEN091** and DMSO-treated samples (N = 1). Maximal and minimal ratios were manually set to 5 and 0.05, respectively.

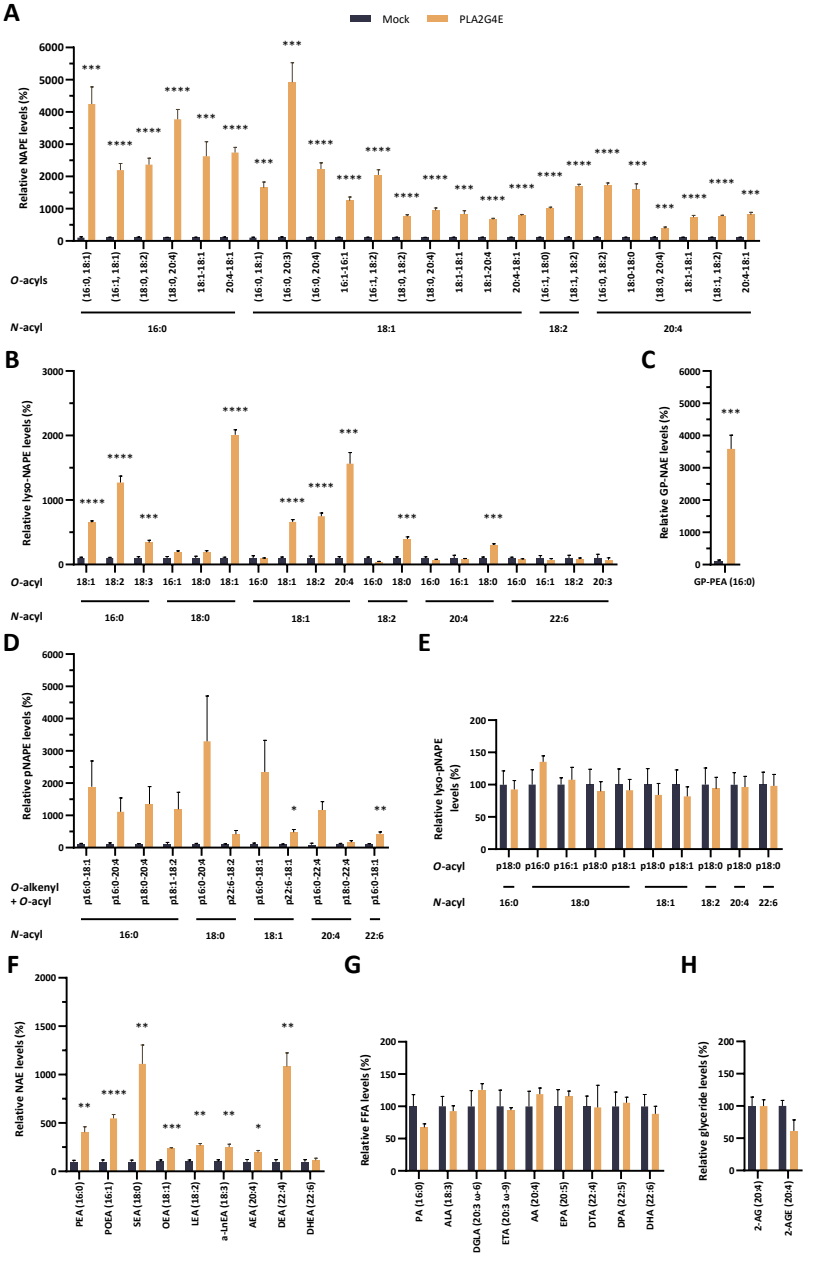

Supplementary Figure S3.4. Lipid level changes in Neuro-2a cells overexpressing PLA2G4E. Relative lipid levels in hPLA2G4E-transfected Neuro-2a cells expressed as percentage compared to mock-transfected cells (24 h p.t.). For individual NAPEs (A) parentheses indicate that the absolute *sn* configuration of the *O*-acyls was not determined. Data expressed as mean ± SEM (N = 5). Statistical significance calculated for each lipid using a two-tailed *t*-test with Holm-Sidak multiple comparison correction. *p < 0.05, **p < 0.01, ***p < 0.001, ****p < 0.0001. PEA: *N*-palmitoylethanolamine, POEA: *N*-palmitoleoylethanolamine, SEA: *N*-stearoylethanolamine, OEA: *N*-oleoylethanolamine, LEA: *N*-linoleoyl-ethanolamine, α-LnEA: *N*-α-linolenoylethanolamine, AEA: *N*-arachidonoylethanolamine, DEA: *N*-docosatetraenoyl-

ethanolamine, DHEA: *N*-docosahexaenoylethanolamine (synaptamide), PA: palmitoic acid, ALA: α-linolenic acid, DGLA: dihomo-γ-linolenic acid, ETA: eicosatrienoic acid (mead acid), AA: arachidonic acid, EPA: eicosapentaenoic acid, DTA: docosatetraenoic acid (adrenic acid), DPA: docosapentaenoic acid, DHA: docosahexaenoic acid, 2-AG: 2-arachidonoyl-glycerol, 2-AGE: 2-arachidonyl glyceryl ether (noladin ether).

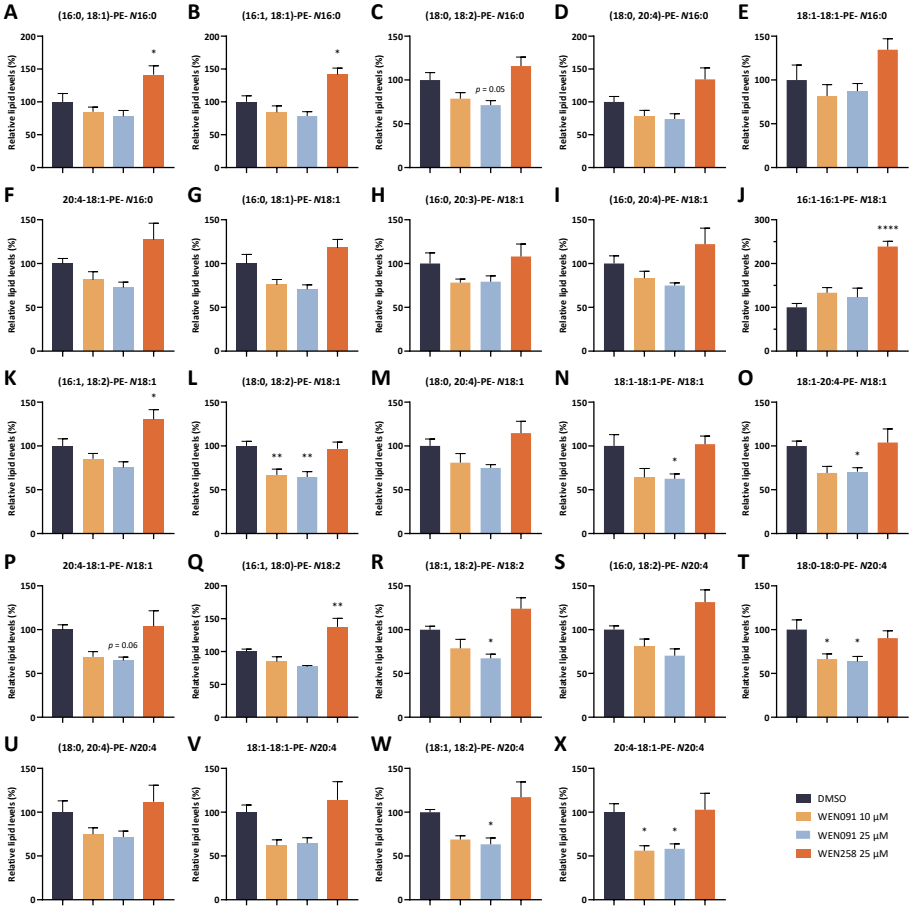

Supplementary Figure S3.5. Relative levels of NAPE species in Neuro-2a cells following inhibitor treatment. Levels determined in PLA2G4E-overexpressing Neuro-2a cells (24 h p.t.) treated with **WEN091**, **WEN258** or vehicle (8 h) expressed as percentage compared to DMSO-treated cells (mean ± SEM, N = 5). Lipid notation as follows: {*sn*-1 *O*-acyl}-{*sn*-2 *O*-acyl}-PE-*N*{*N*-acyl}. Parentheses indicate that the absolute *sn* configuration of the *O*-acyls was not determined. Statistical significance calculated for each lipid using one-way ANOVA with Dunnett's multiple comparison correction. **p* < 0.05, ***p* < 0.01.

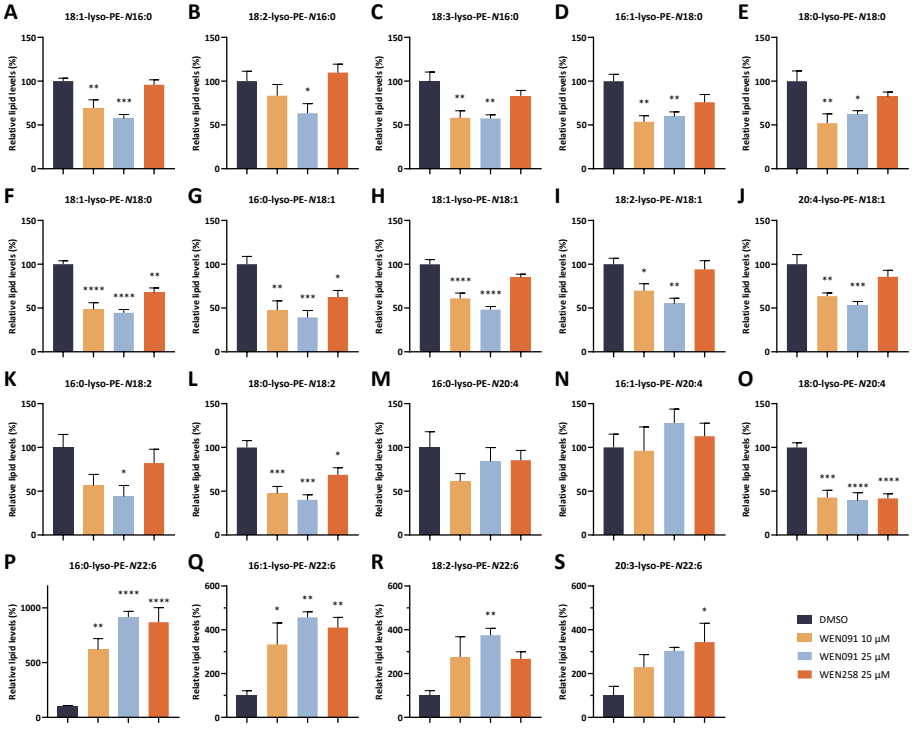

Supplementary Figure S3.6. Relative levels of lyso-NAPE species in Neuro-2a cells following inhibitor treatment. Levels determined in PLA2G4E-overexpressing Neuro-2a cells (24 h p.t.) treated with **WEN091**, **WEN258** or vehicle (8 h) expressed as percentage compared to DMSO-treated cells (mean ± SEM, N = 5). Lipid notation as follows: {*O*-acyl}-lyso-PE-*N*{*N*-acyl}. Statistical significance calculated for each lipid using one-way ANOVA with Dunnett's multiple comparison correction. *$p < 0.05$, **$p < 0.01$, ***$p < 0.001$, ****$p < 0.0001$.

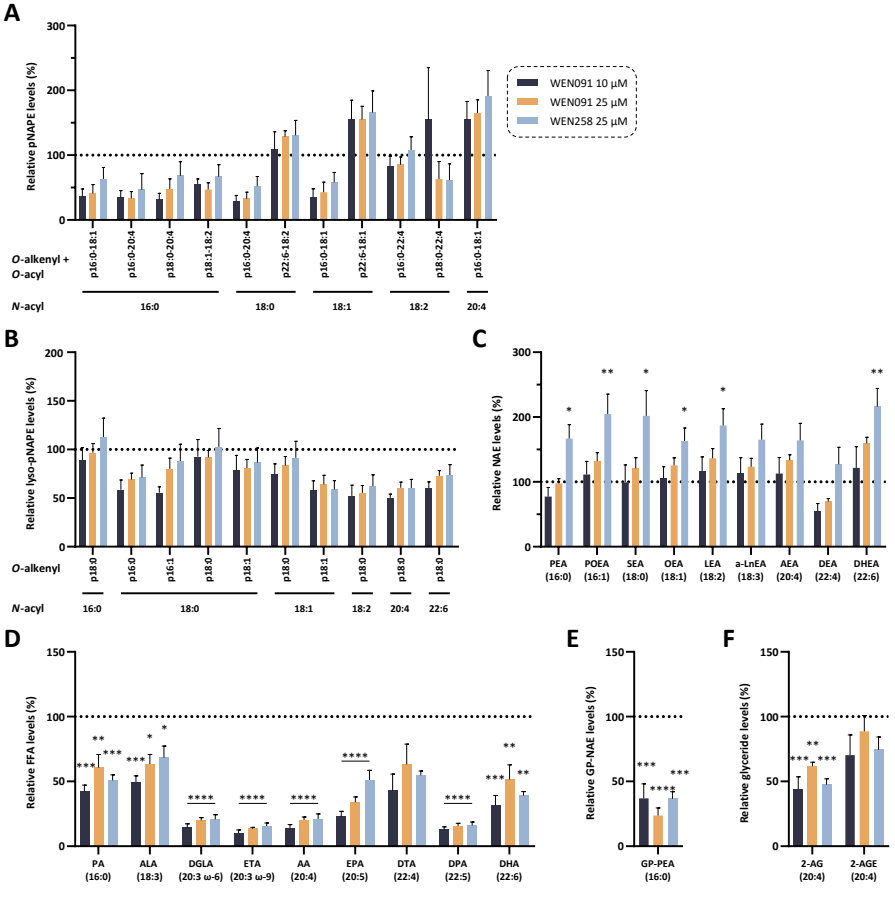

Supplementary Figure S3.7. Relative levels of lipid species in Neuro-2a cells following inhibitor treatment. Levels of (A) pNAPEs, (B) lyso-pNAPEs, (C) NAEs, (D) FFAs, (E) GP-NAEs and (F) glycerides determined in PLA2G4E-overexpressing Neuro-2a cells (24 h p.t.) treated with **WEN091**, **WEN258** or vehicle (8 h) expressed as percentage compared to DMSO-treated cells (mean ± SEM, N = 5). Statistical significance calculated for each lipid using one-way ANOVA with Dunnett's multiple comparison correction. *p < 0.05, **p < 0.01, ***p < 0.001, ****p < 0.0001.

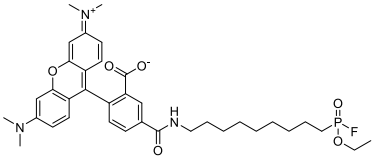

FP-TAMRA

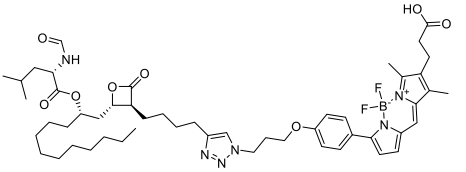

MB064

Supplementary Figure S3.8. Chemical structures of the two activity-based probes used in this study. Commercially available broad-spectrum serine hydrolase probe FP-TAMRA and in-house synthesized tetrahydrolipstatin-based lipase probe MB064.